The Astronomical Journal, 133:2072–2086, 2007 May

SPITZER OBSERVATIONS OF NGC 2362: PRIMORDIAL DISKS AT 5 Myr

S. E. Dahm[1] and L. A. Hillenbrand[1]

Received 2006 August 6; accepted 2006 December 14

ABSTRACT

We present results from a mid-infrared imaging survey of the ∼5 Myr old cluster NGC 2362 carried out with the Infrared Array Camera (IRAC) on board the *Spitzer Space Telescope*. The archival mid-infrared data were merged with extant Hα emission data, optical and near-infrared photometry, and moderate-resolution optical spectroscopy to identify the remnant disk-bearing population of the cluster and to estimate the fraction of stars that still retain primordial circumstellar disks. The principal sample of 232 suspected cluster members with masses ranging from ∼10 to 0.3 $M_{\odot}$ (B2–M5 spectral types) was drawn from known Hα emission stars, X-ray-detected stars from a single 100 ks archival *Chandra* observation, and established lithium-rich stars. A second sample of 153 stars over a similar mass range whose membership status was based on optical photometry alone was also examined. Measured fluxes in the optical and infrared passbands were fitted with synthetic, low-resolution spectra created using the NextGen atmospheric models, permitting the detection of infrared excesses relative to predicted stellar photospheric fluxes. Using the measured slope of the stellar spectral energy distribution through the four IRAC channels to characterize disk emission for the 195 out of 232 activity/lithium-selected stars and the 105 out of 153 photometric membership candidates having complete IRAC photometry, we derive an upper limit for the primordial, optically thick disk fraction of NGC 2362 of ∼7% ± 2%, with another ∼12% ± 3% of suspected members exhibiting infrared excesses indicative of weak or optically thin disk emission. The presence of circumstellar disks among candidate members of NGC 2362 is strongly mass-dependent, such that no stars more massive than ∼1.2 $M_{\odot}$ exhibit significant infrared excess shortward of 8 μm. An upper limit for the fraction of stars hosting primordial, optically thick disks peaks near 10.7% ± 4% for stars with masses between 1.05 and 0.6 $M_{\odot}$, but the *Spitzer* IRAC survey is sensitivity-limited below ∼0.3 $M_{\odot}$. From Hα emission-line strengths, an upper limit for the accretion fraction of the cluster is estimated at ∼5%, with most suspected accretors associated with primordial, optically thick disks identified with *Spitzer*. The presence of primordial disk-bearing stars in NGC 2362, some of which are suspected of still experiencing gaseous accretion, may imply that even within dense cluster environments, sufficient numbers of inner disks survive to ages consistent with core accretion models of giant planet formation to account for the observed frequency of exoplanets within 5 AU of all FGKM-type stars.

Key words: accretion, accretion disks — open clusters and associations: individual (NGC 2362) — stars: formation — stars: pre–main-sequence

Online material: machine-readable tables

1. INTRODUCTION

The current paradigm of circumstellar disk evolution for young, low-mass stars suggests that molecular gas and dust are rapidly cleared from the inner (<5 AU) disk region by planet formation, photoionizing UV and soft X-ray flux, and magnetospheric accretion flows, which channel gas from the inner disk edge to the stellar surface while spreading dust and gas radially outward to conserve angular momentum. From their near ubiquitous presence among the ∼1 Myr old population of the Orion Nebula cluster (inner disk fractions of 55%–90%; Hillenbrand et al. 1998; Lada et al. 2000; Haisch et al. 2001), the frequency of inner disks declines rapidly, to ∼12% in the 5 Myr old cluster NGC 2362 (Haisch et al. 2001). Early ground-based, near-infrared (NIR) observations, however, were sensitive to only the innermost disk regions (≪1 AU), where the stellar photospheric contribution to the observed flux is significant. Capable of probing circumstellar dust beyond the inner 5 AU of disk structure, the *Spitzer Space Telescope* is revolutionizing disk evolution studies. Silverstone et al. (2006) derived the inner (<3 AU) disk fraction of young (3–10 Myr), nearby solar analogs using the *Spitzer* Infrared Array Camera (IRAC), finding that only 5 of 74 stars (∼7%) exhibit strong 3.6–8.0 μm excess. Carpenter et al. (2006) find that 19% of the K- and M-type members of the 5 Myr old Upper Scorpius OB association retain optically thick primordial disks, while <1% of more massive stars exhibit similar infrared excesses. By 10 Myr the inner disk fraction is reduced to <4% as inferred from IRAC observations of NGC 7160 by Sicilia-Aguilar et al. (2006). Dust grain growth, Poynting-Robertson drag, and radiation pressure should theoretically deplete circumstellar dust over timescales of a few megayears (Natta et al. 2007). Circumstellar debris disks, however, persist long after the dissipation of primordial accretion disks, as evidenced by the prominent 12^{+8}_{-4} Myr old debris disks of AU Mic and β Pic (Zuckerman et al. 2001) and the 50 Myr old debris disks found among members of IC 2391 (Siegler et al. 2007). These examples of young debris disks imply that dust regeneration mechanisms such as the collision of planetesimals must periodically replenish the disk.

The principal objective of this investigation is to place constraints on the timescale necessary for primordial circumstellar disks to dissipate and, by inference, for giant planet formation to occur in the terrestrial region. In their review of observed properties of exoplanets, Marcy et al. (2005) state that of 1330 FGKM-type stars examined, 6.6% host giant planets within 5 AU. Extrapolating this lower limit, they conclude that ∼12% of all

[1] Department of Astronomy, California Institute of Technology, Pasadena, CA 91125, USA.

FGK-type stars possess a giant planet within 20 AU. This fraction, while strongly metallicity-dependent, suggests that although not ubiquitous, giant planet formation is certainly not rare. Because the physical mechanism responsible for the genesis and subsequent growth of giant planets is not yet understood, the impact of prolonged primordial disk lifetimes on the probability of giant planet formation is unknown. Two models of giant planet formation have gained preeminence over the last decade: core accretion theory (reviewed by Lissauer 1993) and the disk instability mechanism proposed by Boss (1997). These models are characterized by disparate timescales: 1–10 Myr for the former and ~0.1 Myr for the latter. While incapable of excluding either mechanism, the presence of a substantial population of primordial circumstellar disks (at least approaching the observed frequency of giant planets among field FGKM-type main-sequence stars) in minimally evolved clusters would nullify arguments that timescales required by core accretion theory are inconsistent with the empirically established disk evolution scenario. Given that at least 80% of all stars form within richly populated clusters having 100 members or more (Lada & Lada 2003), disk survival times within these densely populated regions should be representative of those for most stars within the Galactic disk, and very likely that of the Sun.

Lada et al. (2006) recently surveyed the nearby (320 pc), young (2–3 Myr), partially embedded cluster IC 348 with both IRAC and the Multiband Imaging Photometer for *Spitzer* (MIPS) on board *Spitzer*. In their sample of 300 confirmed cluster members from the stellar census of Luhman et al. (2003), Lada et al. (2006) find that 30% ± 4% of the members still retain primordial, optically thick circumstellar disks, and another ~20% of the stars possess weak or optically thin disks. Their classification of disk structure is based on the slope of the spectral energy distribution (SED) relative to that predicted for stellar photospheres. Their findings also imply that disk frequency is spectral type– (or mass-) dependent, peaking near 47% for types K6–M2 and declining to 22% for late-M-type stars. Relative to the strength of Hα emission, a principal accretion indicator, Lada et al. (2006) find that most (68%) classical T Tauri stars (CTTSs) possess optically thick circumstellar dust disks, while only 12% of weak-line T Tauri stars (WTTSs) retain their primordial disks. From these disk fractions of CTTSs and WTTSs in IC 348, Lada et al. (2006) conclude that the presence of dust emission and gaseous accretion are strongly coupled. Similar observations over the full initial mass function in more evolved clusters should further constrain primordial disk lifetimes.

NGC 2362 is a young Galactic cluster dominated by the 4th mag O9 Ib multiple star τ CMa and nearly three dozen B-type stars spherically distributed in a volume ~3 pc in radius. The cluster is free of molecular gas and dust and suffers little ($A_V = 0.31$ mag) interstellar reddening despite a distance of 1.5 kpc (Moitinho et al. 2001). The age of the cluster is assumed to be ~5 Myr (Balona & Laney 1996; Moitinho et al. 2001; Dahm 2005), based on post-main-sequence evolutionary models for τ CMa and by fitting pre-main-sequence isochrones to the substantial low-mass stellar population. The *UBVRI* photometric survey of NGC 2362 by Moitinho et al. (2001) revealed a long, narrow pre–main sequence in the cluster color-magnitude diagram composed of several hundred stars extending from early-A spectral types to near the hydrogen-burning limit. Dahm (2005) identified 130 stars within the cluster exhibiting Hα emission and another 11 stars that show strong Li I λ6708 absorption, but either lacking Hα emission or for which no Hα data were available. The fraction of the T Tauri star population that is composed of weak-line emitters, f(WTTS), is 0.91, compared with 0.53 for the TTS population of IC 348 (Herbig 1998), suggesting that significantly fewer stars are undergoing active accretion at 5 Myr compared to 2–3 Myr. The range in spectral type for the T Tauri populations of the two clusters are different, however, with several G-type members of IC 348 exhibiting Hα emission (Lada et al. 2006), whereas the earliest T Tauri member of NGC 2362 is of K1 type.

In this work we present results of near- and mid-infrared imaging of NGC 2362 that were undertaken with IRAC on board the *Spitzer Space Telescope*. The IRAC wavelength coverage from 3.6 to 8.0 μm is sensitive to dust emission originating from the innermost regions ($\ll$1 AU) of the circumstellar disk out to ~3 AU, assuming a solar-type central star. Over 230 candidate cluster members ranging in spectral type from early B to mid-M have been identified based on Hα emission, detected X-ray flux from a single, deep integration from the *Chandra X-Ray Observatory*, or the presence of strong Li I λ6708 absorption in moderate-resolution spectra obtained with the Gemini Multi-Object Spectrograph (GMOS) on Gemini-North. An additional 153 stars that possess luminosities and colors consistent with cluster membership comprise a second sample. Optical (VR_CI_C) and NIR (JHK) photometry from Dahm (2005) and the Two Micron All Sky Survey (2MASS) are combined with the *Spitzer* IRAC photometry to produce SEDs for both groups of candidate cluster members, which are compared with synthetic spectra generated using the NextGen stellar atmosphere models of Hauschildt et al. (1999). Infrared emission in excess of normal stellar photospheres is then used to identify disk-bearing stars, which are subsequently classified as primordial or weak using the IRAC SED slope criteria of Lada et al. (2006). The accretion fraction of the cluster is estimated from emission strengths of Hα using the classical 10 Å demarcating equivalent width and the spectral type–dependent criteria of White & Basri (2003). Stellar masses are derived for suspected cluster members ($M_* \leq 1.4\ M_\odot$) using the pre-main-sequence, solar-metallicity models of Baraffe et al. (1998). The cluster disk fraction is then examined as a function of stellar mass and compared with the results of Lada et al. (2006) in the younger IC 348 and with Carpenter et al. (2006) in the comparably aged Upper Scorpius OB association.

2. OBSERVATIONS

2.1. *Spitzer IRAC Observations of NGC 2362*

The *Spitzer Space Telescope* mapped the cluster region under program ID 37 (principal investigator [PI]: G. Fazio) using IRAC in a shallow 7 × 6 mosaic, with individual field centers separated by ~4.8′. Each pointing within the mosaic was imaged in the 12.4 s high dynamic range mode, which generates two exposures of 0.4 and 10.4 s. The mapping was performed twice, with an offset of several arcseconds introduced between iterations. The maps are centered near R.A. = $7^{\rm h}18^{\rm m}48.00^{\rm s}$, $\delta = -24^\circ57'00.0''$ (J2000.0), just east of the brightest cluster member, τ CMa. The nominal pixel size for IRAC after application of pixel area corrections is ~1.22″, yielding a field of view of ~5.2′. The basic calibrated data (BCD) images for all four IRAC channels were downloaded from the *Spitzer* archive after initial processing by the IRAC data pipeline software, version S14.0. Scripts within MOPEX, version 030106, were then used to construct co-added, post-BCD mosaics. Data reduction and analysis were also performed in parallel on the individual flattened and pixel-area-corrected BCD images. Cosmic-ray hits and detector artifacts were identified and removed from the BCD images using routines available in the IDL astronomy library. Point-source extraction was performed on both the MOPEX-generated, post-BCD mosaics and the individual BCD images, with fluxes derived from the

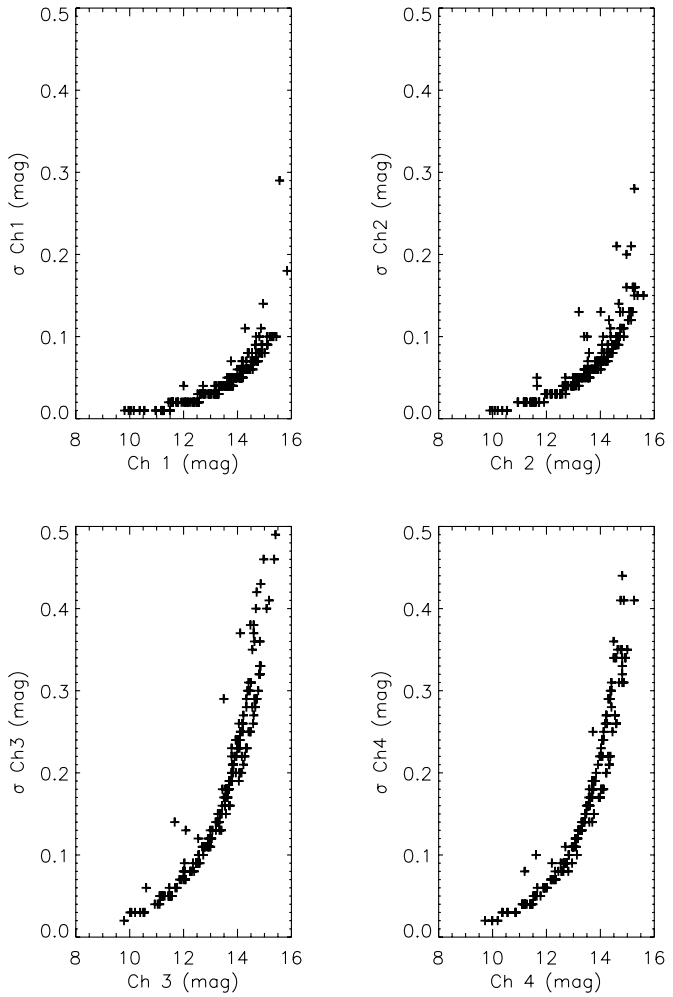

FIG. 1.— Photometric uncertainties for suspected members of NGC 2362 in the four IRAC channels: channel 1 (3.6 μm), channel 2 (4.5 μm), channel 3 (5.8 μm), and channel 4 (8.0 μm).

mosaics taking precedence over those from individual BCD frames. Only when photometry for a given source was not available from the mosaics were the fluxes derived from the BCD image analysis adopted.

Point sources were identified, and aperture photometry was performed on the resulting source lists using the IDL *find.pro* and *aper.pro* routines. Apertures of radii of 2 and 3 pixels were used, with a sky annulus extending from 3 to 7 or 4 to 8 pixels. While the 2 pixel radius aperture is optimal for photometry from a signal-to-noise ratio standpoint, coherent spatial variations in the aperture corrections of 1%–2% across the array are reduced significantly by using a 3 pixel aperture (J. Carpenter 2006, private communication). Multiplicative aperture corrections for the full array of 1.124, 1.127, 1.143, and 1.234 (for the 3 pixel aperture) were applied to the derived fluxes for channels 1, 2, 3, and 4, respectively. The BCD and post-BCD images were flux calibrated in units of MJy sr^{-1}. The derived stellar fluxes were then converted to magnitudes using the flux zero points provided by the *Spitzer* Science Center: 280, 179, 115, and 46 Jy for channels 1, 2, 3, and 4, respectively. Magnitude errors were determined using the standard relation provided by Everett & Howell (2001) for a single measurement. The photometric uncertainties for 220 suspected cluster members with IRAC data available are shown in Figure 1. While 1 σ errors remain <0.2 mag for the entire sample in channels 1 and 2, uncertainties become significant for magnitudes fainter than $\sim$14 in channels 3 and 4. Centered pixel positions for each source identified in the *Spitzer* images were converted to right ascension and declination using astrometry information provided within the headers of the mosaics and the individual BCD images.

2.2. *Optical and Near-Infrared Photometry and Spectroscopy*

The optical (VR_CI_C) and NIR (JHK) imaging and the Wide Field Grism Spectrograph (WFGS) Hα observations of NGC 2362 were obtained using the University of Hawaii 2.2 m telescope on Mauna Kea. The reader is referred to Dahm (2005) for a detailed description of these observations and the procedures followed in their subsequent reduction and analysis. Most (55%) of the 139 Hα emitters (130 from Dahm [2005] and 9 additional emitters from this investigation) in NGC 2362 were detected by the WFGS observations of the cluster made in 2003 January using the Orthogonal Parallel Transfer Imaging Camera (Tonry et al. 1997). These observations are limited to the central 11′ of the cluster core, but are sufficiently deep to detect weak emission from low-mass ($\sim$0.25 $M_\odot$) cluster members (Dahm 2005). The remaining Hα emitters were identified from moderate-resolution spectra obtained for $\sim$200 stars using GMOS on Gemini-North (program GN-2004A-Q-8). These stars were specifically targeted on the basis of Hα emission (from the WFGS observations), their placement above the cluster zero-age main sequence (ZAMS) in the ($V - I_C$, V) color-magnitude diagram, or slit placement constraints. The GMOS spectra were obtained with the R831 grating, which provides adequate spectral resolution for the determination of Li I λ6708 line strengths. Additional optical spectra for seven luminous stars (B6–G5) within the cluster were obtained by Herbig and Dahm on 1999 November 7 using the High Angular Resolution Imaging Spectrograph (HARIS) and the Tektronix CCD camera on the University of Hawaii 2.2 m telescope. These low-resolution ($R \sim 700$) spectra covered the wavelength region from 3800 to 5900 Å, optimal for the classification of early-type stars. All basic image reduction and spectral extraction of the HARIS data was completed using the Image Reduction and Analysis Facility. These seven stars were classified using the line strengths of Fe I λ4045, Ca I λ4226, the CH band at 4300 Å, He I λ4471, and Mg II λ4481.

2.3. *Chandra ACIS Observation*

The deep *Chandra* Advanced CCD Imaging Spectrometer (ACIS) observation of NGC 2362 was made on 2003 December 29, observation ID 4469 (PI: S. Murray), with a nominal integration time of 100 ks. The image and its ancillary data were obtained directly from the *Chandra* archive. The CIAO pipeline reduction process identified over 300 X-ray sources in the cluster field, which were then examined individually on the ACIS image to ensure the reality of the detection and on the red Digitized Sky Survey image of the cluster to identify optical counterparts. After discarding spurious detections or sources lacking optical components, 161 X-ray-detected stars remained. X-ray spectral modeling and the derivation of X-ray luminosities for these sources were not undertaken given the limited purview of the present work. With a field of view of $\sim$16.9′ $\times$ 16.9′, the *Chandra* ACIS observation provides the most complete sampling of candidate members in NGC 2362 in terms of spatial area.

3. ESTABLISHING CLUSTER MEMBERSHIP

Field star contamination is a significant concern for photometric surveys of NGC 2362 given its assumed distance of 1480 pc

(Moitinho et al. 2001) and relative proximity to the Galactic plane ($b = -5.58^\circ$). Lacking proper motion analysis for the cluster, we have adopted three well-established discriminants of stellar youth to distinguish candidate cluster members from field star interlopers: Hα emission, X-ray flux, and Li I λ6708 absorption. The presence of at least one of these youth indicators was deemed sufficient to establish possible cluster membership. The classical means of identifying young, low-mass ($<2\ M_\odot$) stars in young clusters or star-forming regions (SFRs) is the detection of Hα emission from either photographic objective prism surveys or slitless grating imaging surveys. While strong Hα emission in TTSs is attributable to accretion processes, weak emission is believed to arise from enhanced chromospheric activity. Dahm (2005) identifies 130 Hα emitters within the cluster, most of which are probable members.

Enhanced X-ray emission is another well-established indicator of stellar youth, with pre-main-sequence stars possessing X-ray luminosities 1–3 orders of magnitude greater than their main-sequence counterparts (Feigelson & Montmerle 1999). The soft X-ray fluxes of CTTSs and WTTSs are widely accepted to originate from enhanced, solar-like coronal activity, while variable hard X-ray emission is attributed to stochastic flare events. Gaseous accretion from the inner disk is not expected to be a significant contributor to the X-ray spectra of CTTSs given the relatively low impact velocities of infalling gas (Calvet & Gullbring 1998). Of the 161 X-ray-detected sources with optical counterparts in NGC 2362, 62 are identified by Dahm (2005) as Hα emitters. Reinspection of the other 99 X-ray sources on the WFGS images resulted in the discovery of nine additional Hα emission stars with measurable W(Hα), as well as six possible emitters. The WFGS spectra for the 84 remaining X-ray sources either exhibited Hα in absorption, exhibited a featureless continuum (possibly filled absorption profiles), or were overlapped or contaminated by the spectra of nearby stars, or the stars were outside of the WFGS survey area. In addition to the low-mass, pre-main-sequence candidates identified by the Hα emission survey, the X-ray-selected sample includes several early-type (B2–A0) main-sequence stars whose X-ray flux probably originates in stellar winds or from unresolved, low-mass companions.

Perhaps the most definitive youth discriminant for low-mass stars is the presence of strong Li I λ6708 absorption. Pre-main-sequence stars are deeply convective, leading to the destruction of lithium as material is circulated to deeper, higher temperature (>2.5 MK) layers of the stellar interior. Consequently, surface lithium abundance serves as an age index for these types of stars. Dahm (2005) identifies $\sim$100 stars in NGC 2362 that exhibit Li I λ6708 absorption in their GMOS spectra. At the spectral resolution provided by GMOS, Li I λ6707.8 is well separated from most nearby Fe I and Ca I lines, with the exception of the weak Fe I λ6707.45 feature. No corrections for this line or for possible optical veiling effects have been applied to the W(6708) values presented here.

Potential contaminants of the Hα- and X-ray-selected samples of NGC 2362 include foreground dMe stars, but as demonstrated by Dahm (2005) their numbers are limited to approximately seven in the WFGS survey of the cluster. Extrapolating for the larger area of the *Chandra* ACIS field of view, we estimate that $\sim$17 dMe interlopers are among the X-ray-detected sample. Given the low foreground extinction toward NGC 2362, the possibility of background contaminants must also be evaluated. Active dwarfs, however, are intrinsically faint, and if beyond the distance of NGC 2362, their placement in the optical color-magnitude diagram should lend suspicion to their membership status. Other potential sources of contamination include much rarer chromospherically active giants, RS CVn binaries, cataclysmic variables, symbiotic variables, and extragalactic sources. Most of these interlopers should be eliminated by examination of the color-magnitude diagram.

In summary, 232 stars were selected as candidate cluster members on the basis of at least one of these three indicators of youth, ranging in spectral type from B2 to M5. Approximately 20% of the stellar sample exhibit all three indicators, while another 36% possess at least two, and the remaining 44% only one (predominantly X-ray- and Hα-selected stars). While by no means complete, this activity/lithium-selected sample represents the best possible collection of main-sequence and pre-main-sequence candidates within NGC 2362. The photometric survey of Dahm (2005), however, identifies 271 stars within 7′ ($\sim$3 pc) of τ CMa that lie on the cluster ZAMS or between the 1 and 10 Myr isochrones of Baraffe et al. (1998) in the color-magnitude diagram that were not detected by either the X-ray or Hα emission surveys. Many (118) of these stars are faint, $V \geq 21$ mag ($\leq 0.3\ M_\odot$), lying well below the apparent detection threshold of either survey. The remaining 153 stars from this photometric sample (including 14 B-type main-sequence stars) comprise a second membership group, which is included in this analysis to ensure completeness over a significant range of stellar mass. Without additional indicators of youth, the cluster membership status for the low-mass members of this photometric sample should be regarded with less certainty than the principal activity/lithium-selected stars.

Table 1 summarizes the results of the IRAC photometric survey for all 232 activity/lithium-selected members, ordered by increasing right ascension (J2000.0). An identification number is assigned in the first column, which is used to identify individual stars throughout this paper. Listed next are the J2000.0 right ascension and declination, with uncertainties of $<0.5''$. The following six columns present the V magnitude, $V - R_C$ and $V - I_C$ colors, J magnitude, and $J - H$ and $H - K_S$ colors. The optical photometry is from the survey of Dahm (2005), while the NIR data are either from the 2MASS point-source catalog or from Dahm (2005), transformed to the 2MASS system. The positions given in Table 1, as well as the optical and NIR photometry, take precedence over those presented by Dahm (2005).[2] The subsequent columns list the IRAC magnitudes for 3.6 (channel 1), 4.5 (channel 2), 5.8 (channel 3), and 8.0 μm (channel 4) with their associated photometric uncertainties. Next are listed W(Hα), W(6708) if present, and the assigned spectral type, if available. If Hα is not observed in emission, notes are provided in the W(Hα) column providing its status (absorption, flat continuum, or possible emission). The final column of Table 1 annotates whether the star was X-ray-detected. Given the distance of NGC 2362 and the relatively shallow *Spitzer* mapping, 195 of the 232 (84%) suspected cluster members possess IRAC photometry in all four IRAC channels. Another 19 stars have available photometry in at least three channels, and 11 more with only two channels. The photometric cutoff in channels 3 and 4 lies near $m_{5.8/8.0} \sim 15$, where uncertainties reach 0.4 mag.

Table 2 presents available data for the 105 stars in the photometric membership sample of 153, which have complete IRAC photometry. Tabulated in order of increasing right ascension are the J2000.0 coordinates, V-band magnitude, $V - R_C$ and $V - I_C$ colors, J-band magnitude, $J - H$ and $H - K_S$ colors, and the four IRAC magnitudes with their associated uncertainties. Optical photometry for the B-type cluster members presented in Tables 1 and 2 was obtained from the literature, given that many of these

[2] Positional errors or misidentifications noted in Table 2 of Dahm (2005) for the following stars have been corrected in Table 1: stars 115, 145, and 213.

TABLE 1

ACTIVITY/LITHIUM-SELECTED MEMBERS OF NGC 2362

Star	R.A. (J2000.0)	Decl. (J2000.0)	V[a]	$V-R_C$[a]	$V-I_C$[a]	J[b]	$J-H$[b]	$H-K_S$[b]	3.6 μm[c]	Error[c]	4.5 μm[c]	Error[c]	5.8 μm[c]	Error[c]	8.0 μm[c]	Error[c]	W(Hα)[d]	W(6708)[e]	Sp. Type[f]	X-Ray[g]
1.....	7 18 19.61	−24 57 18.0	19.43	0.96	2.63	15.22	0.60	0.25	14.13	0.05	14.11	0.07	14.10	0.20	13.88	0.15	...	...	...	X
2.....	7 18 21.73	−24 57 28.1	17.42	0.97	1.77	14.67	0.72	0.18	13.58	0.04	13.59	0.05	13.52	0.14	13.54	0.13	Cont	...	...	X
3.....	7 18 21.82	−24 51 41.5	18.17	1.00	2.22	14.60	0.74	0.28	13.24	0.03	13.06	0.04	12.76	0.10	12.10	0.06	...	...	...	X
4.....	7 18 22.61	−25 01 41.9	19.68	1.15	2.76	15.54	0.63	0.39	14.28	0.05	14.25	0.07	14.18	0.22	14.11	0.18	4.90	0.81:	M3	ND
5.....	7 18 24.05	−24 53 58.9	18.89	1.05	2.47	14.93	0.52	0.40	14.00	0.06	13.85	0.06	13.80	0.18	14.31	0.22	2.45	0.64	M3	X
6.....	7 18 24.05	−24 54 28.3	18.45	0.99	1.95	15.21	0.58	0.19	14.29	0.06	14.27	0.08	14.41	0.28	14.66	0.32	Cont	...	...	X
7.....	7 18 24.51	−24 54 32.3	17.30	0.58	1.05	12.80	0.62	0.25	11.94	0.02	11.93	0.03	11.79	0.06	11.87	0.05	Abs	0.15	K1	X
8.....	7 18 24.76	−24 57 49.5	18.51	1.05	2.10	15.21	0.63	0.32	14.09	0.05	14.14	0.07	14.05	0.19	14.35	0.26	1.91	0.58	M0	ND
9.....	7 18 25.10	−24 54 18.6	...	...	...	14.89	0.67	0.32	13.62	0.04	13.59	0.05	13.68	0.16	13.45	0.12	2.3	...	...	X
10.....	7 18 25.49	−24 52 27.2	20.12	1.03	2.60	15.91	0.68	0.05	14.61	0.06	14.57	0.08	14.29	0.24	15.10	0.30	Cont	...	...	X

NOTES.—Units of right ascension are hours, minutes, and seconds, and units of declination are degrees, arcminutes, and arcseconds. Table 1 is published in its entirety in the electronic edition of the *Astronomical Journal*. A portion is shown here for guidance regarding its form and content.

[a] Optical photometry from Dahm (2005).

[b] NIR photometry from 2MASS or Dahm (2005).

[c] IRAC photometry in magnitudes with associated uncertainties.

[d] W(Hα) in angstroms (a positive value implies emission). (Abs) Hα in absorption; (Bl) WFGS spectrum blended or overlapping; (Cont) no emission or absorption present at Hα, level continuum; (Em) emission probable. Ellipses indicate no available data.

[e] W(6708) in angstroms (from GMOS). (NP) Not present. Ellipses indicate no available data.

[f] Spectral type.

[g] X-ray detection. (X) X-ray detection; (ND) X-ray nondetection.

TABLE 2
PHOTOMETRIC MEMBERSHIP SAMPLE OF NGC 2362

Star	R.A. (J2000.0)	Decl. (J2000.0)	V[a]	$V-R_C$[a]	$V-I_C$[a]	J[b]	$J-H$[b]	$H-K_S$[b]	3.6 μm[c]	Error[c]	4.5 μm[c]	Error[c]	5.8 μm[c]	Error[c]	8.0 μm[c]	Error[c]
233.....	7 18 17.88	−24 54 34.0	20.47	1.06	2.83	16.54	0.82	0.77	14.98	0.08	14.91	0.10	15.15	0.40	14.71	0.22
234.....	7 18 20.46	−24 55 49.0	14.98	0.39	0.79	13.63	0.36	0.11	13.12	0.03	13.12	0.04	13.18	0.12	13.29	0.11
235.....	7 18 21.20	−24 54 01.2	15.81	0.57	1.17	13.73	0.55	0.17	12.94	0.03	12.92	0.04	12.87	0.10	13.12	0.10
236.....	7 18 22.33	−24 52 13.4	18.35	0.97	2.20	14.90	0.61	0.36	13.85	0.04	13.94	0.06	13.82	0.17	13.83	0.15
237.....	7 18 23.83	−24 55 51.3	19.62	1.06	2.73	15.36	...	...	14.25	0.05	14.08	0.06	14.01	0.17	13.76	0.13
238.....	7 18 25.20	−25 00 37.5	15.91	0.70	1.28	13.81	0.56	0.18	13.01	0.03	12.99	0.04	13.03	0.11	13.03	0.09
239.....	7 18 25.21	−24 54 18.6	18.88	1.06	2.57	14.89	0.67	0.32	13.62	0.04	13.59	0.05	13.68	0.16	13.45	0.12
240.....	7 18 25.24	−24 57 03.0	19.60	1.00	2.42	15.63	0.53	0.21	14.55	0.06	14.40	0.07	14.44	0.25	14.35	0.20
241.....	7 18 25.52	−24 53 26.0	15.37	0.62	1.12	13.48	0.52	0.10	12.76	0.03	12.81	0.04	12.76	0.09	12.88	0.10
242.....	7 18 26.46	−24 56 11.3	16.94	0.73	1.40	14.53	0.54	0.21	13.65	0.04	13.79	0.06	13.75	0.17	13.88	0.15

NOTES.—Units of right ascension are hours, minutes, and seconds, and units of declination are degrees, arcminutes, and arcseconds. Table 2 is published in its entirety in the electronic edition of the *Astronomical Journal*. A portion is shown here for guidance regarding its form and content.
[a] Optical photometry from Dahm (2005).
[b] NIR photometry from 2MASS or Dahm (2005).
[c] IRAC photometry in magnitudes with associated uncertainties.

luminous stars were saturated on the VR_CI_C-band images of Dahm (2005).

4. THE COLOR-MAGNITUDE DIAGRAM OF SUSPECTED CLUSTER MEMBERS

Shown in Figure 2 is the extinction-corrected $(V-I_C, V)$ color-magnitude diagram for the subset of suspected cluster members from Table 1 with detected Hα emission, X-ray emission, or Li I λ6708 absorption having available optical photometry (200 out of 232). Also shown are the 153 stars from the photometric membership sample. The dwarf colors of Kenyon & Hartmann (1995) were used to place the B-type stars on the near-vertical portion of the cluster ZAMS. Notably missing is τ CMa, which although detected by *Chandra* is saturated on the optical images of Dahm (2005). To correct for interstellar and local extinction effects, we use spectral types from Dahm (2005) and the literature to determine

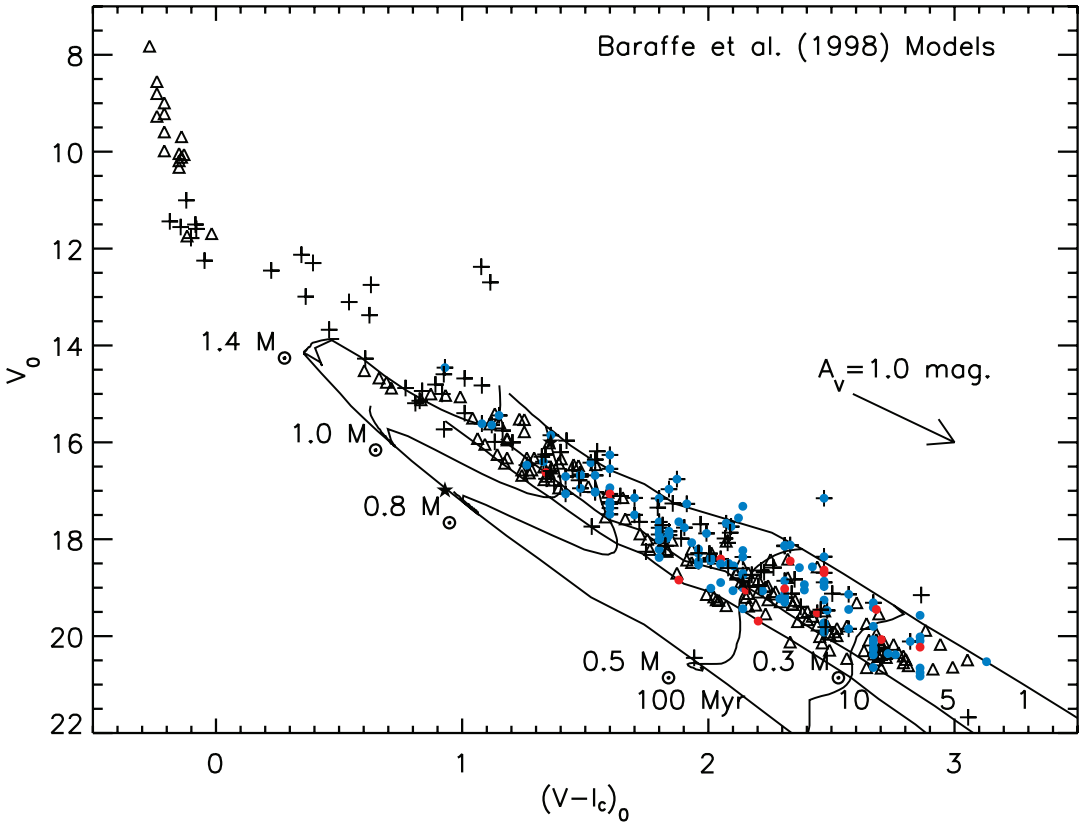

FIG. 2.—Extinction-corrected $(V-I_C, V)$ color-magnitude diagram for ~200 suspected members of NGC 2362 with detected Hα emission, X-ray emission, or Li I λ6708 absorption. Filled red circles denote Hα emitters with strong emission, W(Hα) $\geq$ 10 Å (CTTSs), filled blue circles represent those Hα emitters with weak emission, W(Hα) < 10 Å (WTTSs), crosses represent X-ray-detected stars (many of which also exhibit Hα emission), and five-pointed stars show pre-main-sequence candidates with detectable Li I λ6708 absorption but lacking both Hα and X-ray emission (or available data). Open triangles represent the 153 additional candidate members of NGC 2362 based on optical photometry alone. All of these stars possess V-band magnitudes <21, lie between the 1 and 10 Myr isochrones of Baraffe et al. (1998), and are within 7′ (~3 pc) of τ CMa. The 1, 5, 10, and 100 Myr isochrones, as well as the 0.3, 0.5, 0.8, 1.0, and 1.4 $M_\odot$ evolutionary tracks of Baraffe et al. (1998), are superposed.

A_V values from color excesses, assuming a normal reddening relationship of $A_V = 3.08E(B-V) = 2.43E(V-I_C)$. For stars of unknown spectral type, we adopt the mean cluster $E(B-V)$ value given by Balona & Laney (1996) and Moitinho et al. (2001), $E(B-V) = 0.10$, corresponding to $A_V \approx 0.31$ mag. Superposed in Figure 2 are the evolutionary tracks and isochrones of Baraffe et al. (1998). These models are limited to ages between 1 Myr and several gigayears and to masses $\leq 1.4\ M_\odot$. The effective temperatures ($T_{\rm eff}$) and luminosities predicted by the Baraffe et al. (1998) models were transformed to the observational plane using the main-sequence relationships between bolometric correction and the $T_{\rm eff}$ and $V-I_C$ color of Hillenbrand (1997).

Most of the activity/lithium-selected stars lie between the 1 and 10 Myr isochrones of the Baraffe et al. (1998) models, with the earliest spectral types, above the 1.4 $M_\odot$ evolutionary track, being concentrated around the cluster ZAMS. The placement of some stars in the color-magnitude diagram, however, brings to question their membership status. One X-ray-detected WTTS (star 109 of Table 1) lies well above the earliest isochrone of the Baraffe et al. (1998) models, near $V-I_C \approx 2.45$. The GMOS spectrum of this star reveals an M3 spectral type, but Li I λ6708 is not present. The He I λ5876 chromospheric line, however, is in weak emission, suggesting that the star could be a field dMe interloper. Two luminous ($V \sim 12.5$), X-ray-detected stars (stars 28 and 166) also lie well above the locus of suspected members. Spectra are not available for these stars, but their $V-I_C$, $V-K_S$, and $J-K_S$ colors imply early to mid-K spectral types, suggesting that these are likely foreground dwarfs. Two additional stars are worth mention here, the lithium-rich star lying below the 100 Myr isochrone of Baraffe et al. (1998), near the terminus of the 0.8 $M_\odot$ evolutionary track, and the X-ray-detected star also below the 100 Myr isochrone, lying near the terminus of the 0.5 $M_\odot$ track. The former (star 7) is an early K-type star and a close visual double. Although point-spread function (PSF) fitting photometry was performed, photometric errors may contribute to its odd placement. It is also possible that spectral contamination occurred in the moderate seeing conditions present (1″) during the GMOS data acquisition. The latter faint X-ray source (star 39) exhibits a broadened PSF in the optical and is possibly a background galaxy. Numerous other background galaxies were noted by Dahm (2005) in the optical and NIR images of NGC 2362, which is apparently superposed on a galaxy cluster. All other pre-main-sequence candidates, based on their location in the ($V-I_C$, V) color-magnitude diagram, are consistent with being cluster members. The aforementioned stars with anomalous locations, however, were excluded from the disk analysis of the cluster population.

The stars of the photometric membership sample are predominantly positioned either below the 0.5 $M_\odot$ evolutionary track in Figure 2 where completeness impacts the activity/lithium-selected sample, or above the 1.0 $M_\odot$ track where the number of potential field interlopers increases significantly. For $13.0 \leq V \leq 16.5$ the cluster sequence approaches and passes through the locus of the field stellar population in the ($V-I_C$, V) color-magnitude diagram (see Fig. 2 of Dahm 2005). Between the 0.5 and 1.0 $M_\odot$ evolutionary tracks of Baraffe et al. (1998), however, it is apparent that the activity/lithium selection criteria performed well in identifying probable cluster members. Combining both cluster membership samples, we find that two gaps in mass coverage remain: below 0.3 $M_\odot$ where the IRAC survey is sensitivity-limited and within the range from 1.4 to 3 $M_\odot$ (late-F through early-A spectral type), where field star contamination is significant, making membership determination based on photometry alone problematic.

5. SPECTRAL ENERGY DISTRIBUTIONS AND DISK EMISSION

To identify cluster members with infrared excesses indicative of circumstellar disks, SEDs spanning the wavelength range from 0.54 to 8.0 μm were produced using the optical and infrared photometry of Tables 1 and 2. These observed SEDs were then compared with synthetic spectra generated using the NextGen stellar atmospheric models of Hauschildt et al. (1999). Solar metallicities and dwarflike surface gravities ($\log g = 5$) were adopted to generate the model stellar photospheres. The NextGen models are valid over an effective temperature range from 3000 to 10,000 K at a resolution of 200 K, adequate coverage and granularity for the majority of pre-main-sequence candidates in NGC 2362. The main-sequence $T_{\rm eff}$ values compiled by Kenyon & Hartmann (1995) were assumed for stars of known spectral type. If the spectral types were unknown, the cluster mean extinction was adopted to determine an intrinsic $V-I_C$ color and its corresponding spectral type. After extinction corrections and the application of a distance correction factor, the stellar SEDs were fitted in the optical and NIR passbands, where disk emission is minimized, to the synthetic photospheric spectra.

To characterize possible disk emission, the slope of the SED through the IRAC passbands was determined for each suspected cluster member. This slope, α, defined by Lada & Wilking (1984) and Lada (1987) as $\alpha = d\log(\lambda F_\lambda)/d\log(\lambda)$, was determined from a linear regression fit of the derived fluxes in the four IRAC channels. These slopes range from -3.83 to -0.18 and were compared to metrics established by Lada et al. (2006) in their examination of the pre-main-sequence population of IC 348. The SEDs of stellar photospheres, i.e., diskless stars, are characterized by a slope of $\alpha < -2.56$, which corresponds to the modeled photosphere of an M0-type dwarf. The IRAC wavelength range is on the Rayleigh-Jeans tail of the stellar photosphere SED, leading to similar intrinsic colors for all spectral types. Among candidate members of NGC 2362, there is a continuum of slopes with a clustering toward values expected of stellar photospheres. For our sample of B2–M5 stars, the mean α for stars lacking evidence for disk emission is -2.85, with a standard deviation of 0.17. For the disk candidates in IC 348, Lada et al. (2006) compare the observed SEDs to two radiative transfer disk models that assume a $\Sigma \sim r^{-1}$ surface density profile, but of varying scale height. From their analysis, they conclude that observed SEDs matching the disk models are best represented by $\alpha \geq -1.80$. These stars are assumed to host optically thick or primordial circumstellar disks. They define "anemic" disk systems as being characterized by slopes between these extrema, $-2.56 < \alpha < -1.80$. Such weak disks may represent transitional disk systems with inner disk gaps cleared out by dust grain growth, planet formation, or photoevaporation by UV and FUV flux. Uncertainties inherent in the use of α arise from both flux measurement errors and the nonlinear SED profiles of disk-bearing stars. Furlan et al. (2006) find a broad range of SED morphologies in their 5–36 μm *Spitzer* Infrared Spectrograph survey of T Tauri stars in Taurus-Auriga. The diversity among their morphological sequence of Class II sources emphasizes the limited ability of simple linear fits to categorize disk structure. Degeneracy among IRAC slope values for very different SED profiles may cause misclassifications of circumstellar disk emission. As an example, a disk-bearing candidate with near photospheric emission out to 5.6 μm may exhibit a sharp rise at 8 μm possibly associated with the 10 μm silicate emission feature. From the slope of its SED, this disk may be categorized as primordial, but such silicate emission without evidence for significant

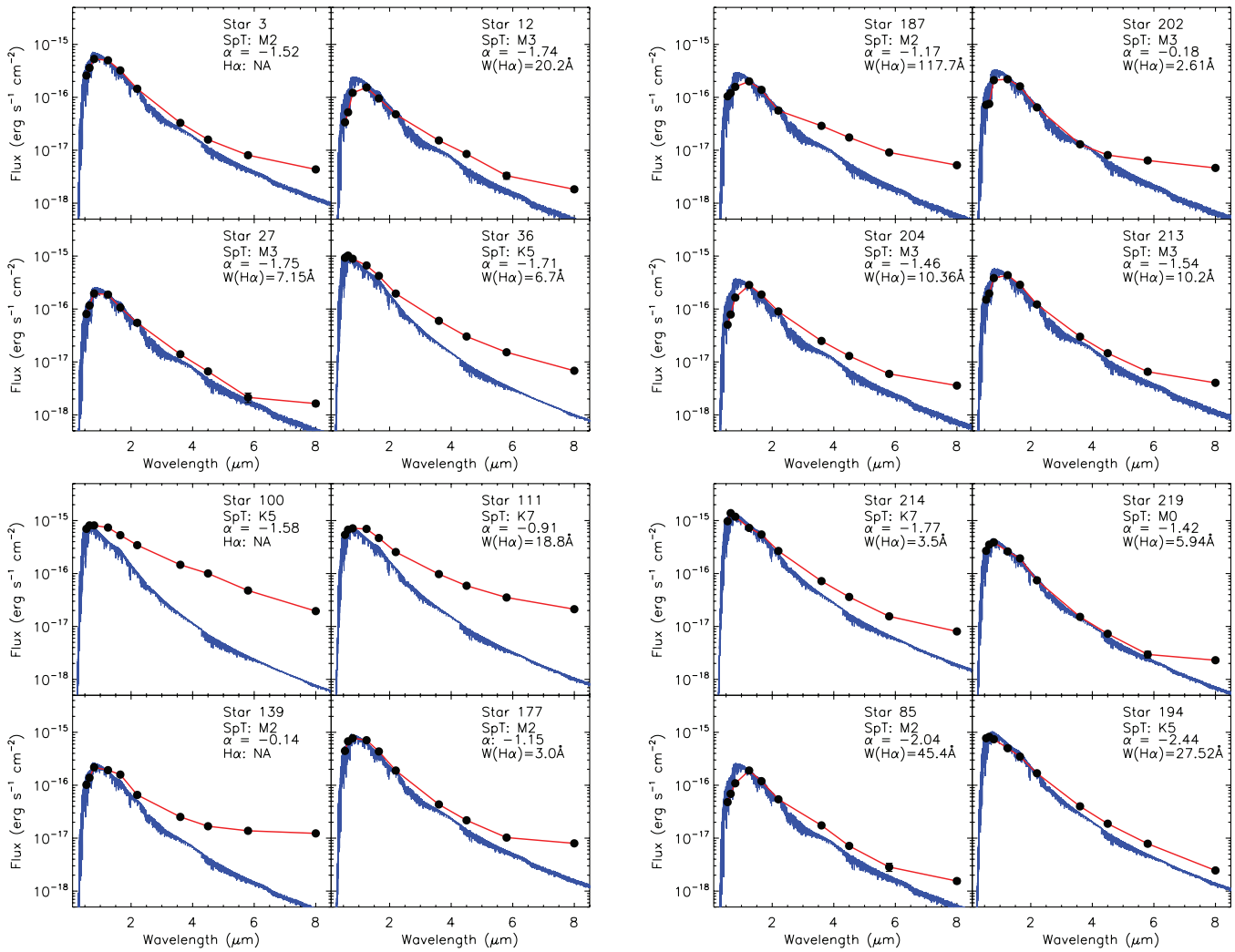

FIG. 3.—SEDs for all suspected primordial disk candidates in NGC 2362 shown with the NextGen stellar atmospheric model of the nearest available spectral type superposed in blue. Uncertainties for the optical and infrared photometry are overplotted, but in most cases are contained within the boundaries of the plotting symbols. In the upper right corner of each SED the stellar identifier is given (from Table 1) with the slope parameter α, the spectral type of the fitted photosphere, and $W(\mathrm{H}\alpha)$ if emission is present. The final two SEDs shown (stars 85 and 194) are suspected accretors based on $W(\mathrm{H}\alpha)$ and the criteria of White & Basri (2003) but exhibit weak disk emission.

continuum excess at shorter wavelengths implies a disk that is very likely optically thin in nature.

Acknowledging the possible limitations of the IRAC SED analysis to distinguish between classes of disk structure, we adopt the metrics established by Lada et al. (2006) in order to compare directly the observed excess stars in NGC 2362 with those in IC 348. Using identical boundary conditions, we find 14 stars, of the 195 examined from the activity/lithium-selected membership sample having complete IRAC photometry, with primordial disk emission and another 24 stars with suspected weak disk emission. From the activity/lithium-selected sample, we place an upper limit on the primordial, optically thick disk fraction of the cluster of $\sim 7\% \pm 2\%$, while another $\sim 12\% \pm 3\%$ of suspected members exhibit infrared excesses indicative of weak disk emission. The errors presented reflect simple Poisson statistical uncertainties.

Of the 153 stars in the photometric membership sample of NGC 2362, 105 have measured fluxes in all four IRAC channels. While no additional primordial disks were identified in this sample, nine stars, all of which lie below the 0.5 $M_{\odot}$ evolutionary track of Baraffe et al. (1998), were found to exhibit possible weak disk emission. If these 105 photometric membership candidates are included in the cluster disk-bearing statistics, the primordial disk fraction of NGC 2362 is reduced to $\sim 5\%$, while the weak disk fraction decreases slightly to $\sim 11\%$. In summary, just under 20% of all candidate members of NGC 2362 exhibit infrared excess shortward of 8 μm, indicative of dust emission within the terrestrial region. While both membership samples are certainly incomplete for lower masses ($\leq 0.3\ M_{\odot}$), this inner disk fraction is significant for stars with masses between ~ 0.5 and 1.2 $M_{\odot}$, where the cluster population is well sampled by the Hα and *Chandra* surveys.

In Figure 3 the SEDs for the 14 suspected primordial disk candidates are plotted, with the NextGen stellar atmospheric model of the nearest available spectral type superposed in blue. The models have been smoothed to reduce the level of detail present in the synthetic absorption spectra. Uncertainties for the optical and infrared photometry are overplotted, but in most cases the errors are contained within the boundaries of the plotting symbols. In the upper right corner of each SED, the stellar identifier (from Table 1) is given with the slope parameter α, the spectral type of the fitted photosphere, and $W(\mathrm{H}\alpha)$ if emission is present. Table 3 lists the properties of the 47 disk candidates from both membership samples of the cluster, including the IRAC slope parameter and its associated uncertainty, disk classification (primordial or weak), $W(\mathrm{H}\alpha)$

TABLE 3
PROPERTIES OF DISK CANDIDATES IN NGC 2362

Star[a]	α[b]	Disk Type[c]	W(Hα)[d]	Accretion[e]	Mass ($M_\odot$)[f]
3	-1.52 ± 0.21	Primordial	...	...	0.58
12	-1.74 ± 0.26	Primordial	13.55	Yes	0.28
25	-2.39 ± 0.14	Weak	...	...	0.70
26	-2.54 ± 0.07	Weak	...	...	0.56
27	-1.75 ± 0.57	Primordial	7.15	No	0.42
29	-2.27 ± 0.15	Weak	1.94	No	0.78
36	-1.71 ± 0.09	Primordial	6.7	Yes	1.15
39	-2.27 ± 0.03	Weak	...	...	0.51
61	-2.18 ± 0.38	Weak	3.11	No	0.29
76	-2.53 ± 0.34	Weak	5.69	No	0.26
85	-2.04 ± 0.36	Weak	45.4	Yes	0.46
89	-2.51 ± 0.11	Weak	1.09	No	0.68
95	-2.53 ± 0.08	Weak	4.44	No	0.34
100	-1.58 ± 0.17	Primordial	Bl	...	0.89
108	-2.55 ± 0.27	Weak	Bl	...	0.61
111	-0.91 ± 0.11	Primordial	18.8	Yes	0.77
118	-1.87 ± 0.14	Weak	Em?	No	0.58
120	-2.27 ± 0.12	Weak	13.7	No	0.49
139	-0.14 ± 0.22	Primordial	...	...	0.51
145	-2.33 ± 0.12	Weak	2.36	No	0.73
154	-2.51 ± 0.20	Weak	...	...	0.36
158	-2.50 ± 0.21	Weak	6.28	No	0.60
175	-2.35 ± 0.24	Weak	2.82	No	0.32
177	-1.15 ± 0.42	Primordial	3.0	No	0.60
180	-2.41 ± 0.13	Weak	8.36	No	0.35
187	-1.17 ± 0.13	Primordial	117.65	Yes	0.62
192	-2.32 ± 0.11	Weak	9.25	No	0.39
194	-2.49 ± 0.04	Weak	27.52	Yes	1.05
201	-2.53 ± 0.09	Weak	...	...	0.48
202	-0.18 ± 0.24	Primordial	2.61	No	0.37
204	-1.46 ± 0.26	Primordial	10.36	No	0.33
213	-1.54 ± 0.32	Primordial	10.2	No	0.47
214	-1.77 ± 0.02	Primordial	3.5	No	0.80
219	-1.42 ± 0.49	Primordial	5.94	No	0.67
227	-2.16 ± 0.43	Weak	Em	No	0.50
228	-2.19 ± 0.04	Weak	5.4	No	0.46
229	-1.94 ± 0.06	Weak	3.75	No	0.57
230	-2.48 ± 0.11	Weak	1.55	No	0.68
237	-2.30 ± 0.06	Weak	...	...	0.34
251	-2.18 ± 0.08	Weak	...	...	0.29
267	-1.99 ± 0.19	Weak	...	...	0.37
285	-2.52 ± 0.16	Weak	...	...	0.22
287	-2.27 ± 0.27	Weak	...	...	0.27
290	-2.12 ± 0.17	Weak	...	...	0.25
298	-2.33 ± 0.12	Weak	...	...	0.46
299	-2.46 ± 0.34	Weak	...	...	0.24
327	-1.88 ± 0.43	Weak	...	...	0.49

[a] Star number from Table 1.
[b] IRAC SED slope parameter α.
[c] Disk class based on α.
[d] W(Hα) in angstroms (a positive value implies emission). (Bl) WFGS spectrum blended or overlapping; (Em) emission probable. Ellipses indicate no available data.
[e] Accretion activity suspected based on the W(Hα) criteria of White & Basri (2003).
[f] Stellar mass derived from the evolutionary models of Baraffe et al. (1998).

if emission is present, whether the star is a suspected accretor (the reader is referred to § 8), and the mass of the host star (see § 7).

6. INFRARED COLOR-COLOR DIAGRAMS OF NGC 2362

From the ($K - L, J - H$) color-color diagram of NGC 2362, Haisch et al. (2001) concluded that 12% ± 4% of stars with masses >1 $M_\odot$ possessed infrared excess emission indicative of circumstellar dust. Their L-band observations were sensitive to hot (900 K), micron-size grains within the inner (≪1 AU) disk region but were limited by high sky background and strong stellar photospheric contributions at K and L bands. The mid-infrared IRAC photometry is sensitive to dust temperatures ranging from 300 to 1000 K, corresponding to radial distances of ≪1 AU to 3 AU, assuming the disk candidates to be solar analogs. Shown in Figure 4 (*left*) is the ($K_S - 4.5$ μm, $J - H$) color-color diagram for over 550 2MASS point sources within 7′ of τ CMa and having quadrature-added photometric uncertainties of <0.15 mag. Shown in Figure 4 (*right*) is the ($K_S - 4.5$ μm, $J - H$) color-color diagram for stars in both membership samples of NGC 2362 and with quadrature-added photometric uncertainties of <0.15 mag. Symbols used in the figure distinguish stars on the basis of their infrared excesses as determined by the IRAC SED slope parameter. Comparing the left and right panels of Figure 4 we see that few additional infrared excess stars can be identified from the unbiased 2MASS sample that are not already accounted for among the combined samples of probable cluster members. Several stars in Figure 4 (*right*) are not represented in Figure 4 (*left*), as the photometry for these stars is taken from the NIR survey of Dahm (2005).

Significant scatter about the dwarf locus is evident in Figure 4 (*right*), but most suspected cluster members appear concentrated along its vertical trunk or lie just above the branch defined by the M dwarfs. Approximately 20 stars lie to the right of the dwarf reddening boundary, most of which possess primordial or weak circumstellar disks based on the slopes of their IRAC SED profiles. Of the 14 primordial disk candidates, only one, star 219, lies inside the reddening limits of the dwarf locus. The SED of this X-ray-detected, M0-type WTTS with strong Li I absorption exhibits no excess emission blueward of 4.5 μm, but strong 5.8 and 8.0 μm excess. The weak disk candidates in Figure 4 (*right*) are preferentially found within the reddening limits of the dwarf locus, as might be expected for transitional disk systems, but seven (∼22% of the total weak disk population) do possess significant $K_S - 4.5$ μm color excesses, implying that micron-sized dust grains are still present within their inner disks.

Shown in Figure 5 is the IRAC (4.5 μm − 8.0 μm, 3.6 μm − 4.5 μm) color-color diagram for the activity/lithium-selected stars and the photometric membership sample detected at 3.6, 4.5, and 8.0 μm and having photometric uncertainties of <0.3 mag. Error bars are shown for the primordial disk systems, which are representative of the uncertainties for both weak disk systems and nonexcess stars. As might be expected, the stellar population of NGC 2362 forms a near continuous sequence with increasing (4.5 μm − 8.0 μm) color from stars lacking IRAC excesses to weak disk systems, to primordial disk-bearing stars. The IRAC color-color diagrams of NGC 2362 and the younger IC 348 exhibit similar ranges of observed colors for disk classes. The photometric uncertainties, particularly at 8.0 μm, however, are significantly larger for the more distant NGC 2362, as evidenced by the large scatter among the faint, diskless stellar population. Several IRAC nonexcess stars lie within the region occupied by the weak disk candidates, but the quadrature-added photometric uncertainties for these stars are large.

7. THE DEPENDENCE OF CIRCUMSTELLAR DISK FREQUENCY ON STELLAR MASS

The presence of circumstellar disks (primordial or weak) among candidate members of NGC 2362 is strongly mass-dependent, as demonstrated in Figure 6, which plots the logarithm of the ratio

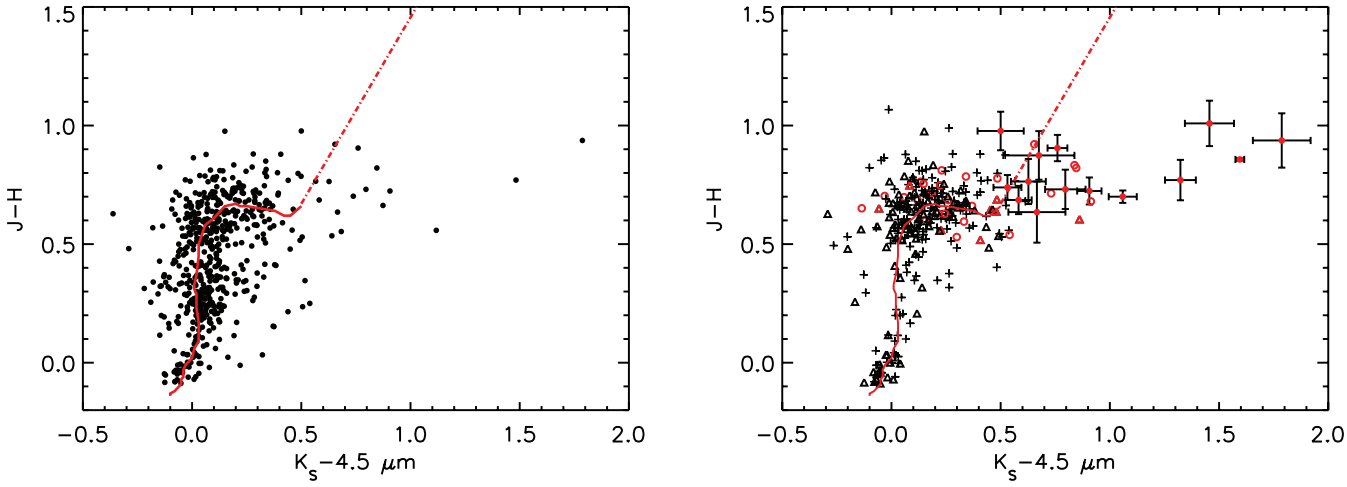

FIG. 4.—*Left*: ($K_S - 4.5$ μm, $J - H$) color-color diagram for 2MASS point sources within 7′ (~3 pc) of τ CMa and having quadrature-added photometric uncertainties of <0.15 mag. The curved solid red line represents the intrinsic colors of normal main-sequence stars, derived from the $J - H$ colors of Tokunaga (2000) and interpolation of the $K_S - 4.5$ μm main-sequence colors of Lada et al. (2006). The red dot-dashed line extending above this curve delineates the approximate reddening boundary for dwarfs, the slope of which was derived using *M*-band extinction curve data from Martin & Whittet (1990). *Right*: ($K_S - 4.5$ μm, $J - H$) color-color diagram for all suspected members of NGC 2362. If primordial disk emission is inferred from the IRAC SED slope parameter α, the star is represented by a solid red circle, if weak disk emission is present the star is shown as an open red circle, and if no excess is detected, by a cross. Stars selected as members based on optical photometry alone and having quadrature-added photometric uncertainties of <0.15 mag are represented by triangles, with those exhibiting weak disk emission in red. Error bars for the primordial disk-bearing candidates are superposed, which are also representative of typical uncertainties for the weak and IRAC nonexcess stellar populations.

of the 8.0 and 4.5 μm fluxes as a function of $J - H$ color, a tracer of stellar photospheric emission. While photometric uncertainties are large for the low-mass stars, leading to significant scatter about the abscissa for $J - H > 0.5$, none of the higher mass stars, which are characterized by small flux errors, exhibit significant excess emission within the IRAC passbands using the adopted SED slope criteria. One possible exception is star 276 from Table 2 (star 39 from Johnson 1950). This B2 main-sequence star was classified as diskless in the IRAC SED slope analysis but appears to have excess 8.0 μm relative to 4.5 μm flux in Figure 6. The models of Hauschildt et al. (1999) are limited to $T_{\rm eff} < 10{,}000$ K, preventing direct comparison with the observed SED. Additional *Spitzer* IRAC and MIPS observations are needed to confirm the presence of disk emission around this early-type star. The apparent lack of optically thick dust emission for stars with $J - H \leq 0.5$ (K2 spectral type) implies that primordial disk evolutionary timescales are significantly longer for stars less massive than ~1.1 $M_\odot$ (the approximate mass of a 5 Myr old K2-type star) than for earlier spectral types. Carpenter et al. (2006) find a similar trend in the 5 Myr old Upper Scorpius OB association in which 19% of the K0–M5 (1.2–0.1 $M_\odot$) stars exhibit 4.5–8.0 μm excesses, while less than 1% of the more massive stars possess such optically thick disk emission.

In their study of IC 348, Lada et al. (2006) find a dependence of disk fraction on stellar mass such that the primordial disk

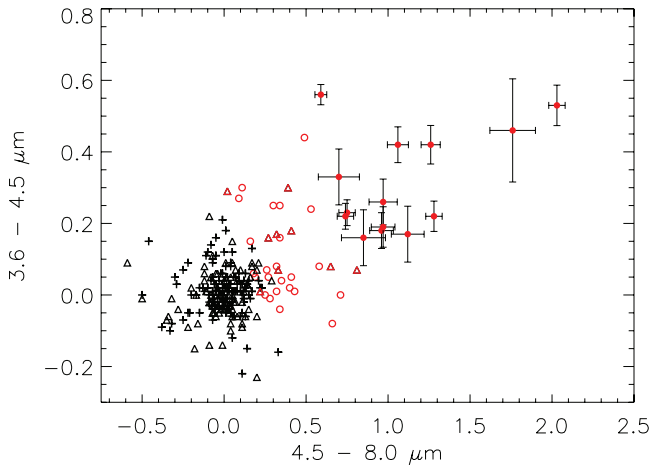

FIG. 5.—IRAC (4.5 μm − 8.0 μm, 3.6 μm − 4.5 μm) color-color diagram for those candidate members of NGC 2362 detected at 3.6, 4.5, 5.8, and 8.0 μm with photometric uncertainties of <0.3 mag. Error bars are shown for the primordial disk systems, which are representative of the uncertainties for both weak disk systems and nonexcess stars. Symbols are as in Fig. 4. The several nonexcess interlopers located within the region occupied by weak disk systems possess large photometric uncertainties, possibly accounting for their placement in the IRAC color-color diagram.

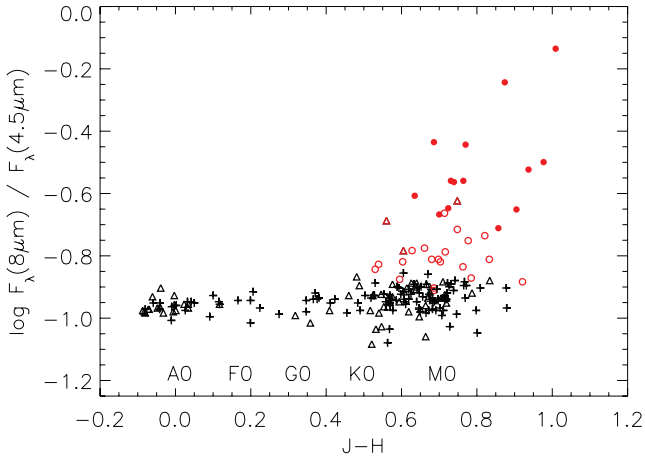

FIG. 6.—IRAC-derived 8.0-to-4.5 μm flux ratio plotted as a function of $J - H$ color for all suspected members of NGC 2362 with 8.0 and 4.5 μm photometric errors of <0.2 mag. Symbols are as in Fig. 4. The larger scatter about the abscissa for the lower mass stars arises from sensitivity limits at 8 μm, which tend to deflect the distribution toward more negative flux ratios. None of the higher mass stars with $J - H \leq 0.5$ (K2 spectral type) exhibit significant infrared excess for $\lambda < 8.0$ μm using the established disk criteria. This result is similar to that of Carpenter et al. (2006) in the 5 Myr Upper Scorpius OB association, in which <1% of the high-mass stars were found with infrared excess shortward of 8.0 μm, while 19% of the K- and M-type members were identified with excess emission in the IRAC channels.

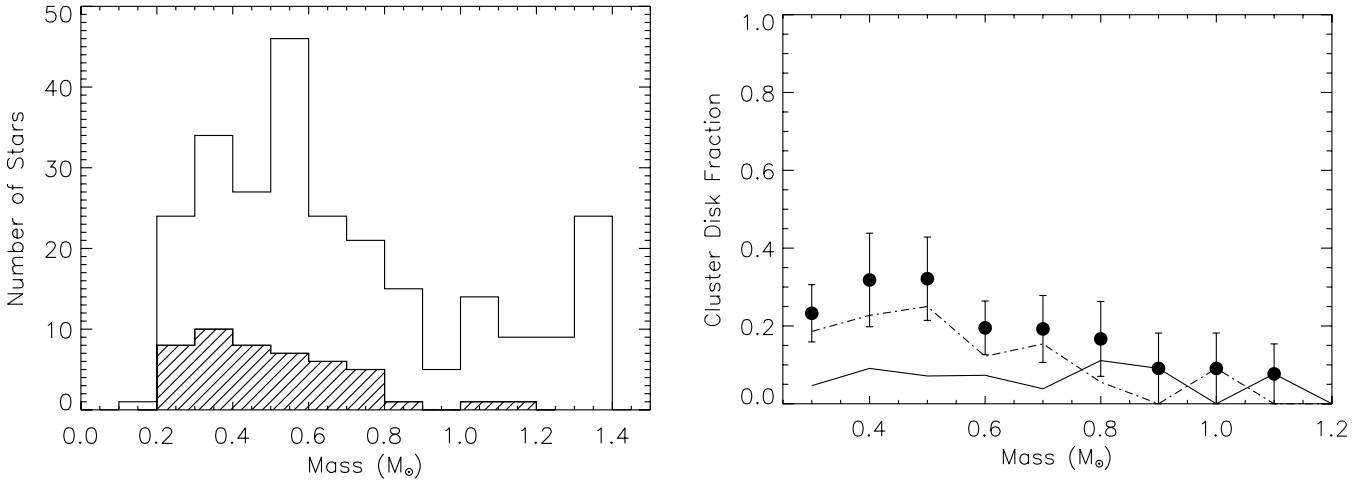

FIG. 7.—*Left*: Mass distribution for 253 candidate cluster members with complete IRAC photometry from Tables 1 and 2 and having masses $\leq 1.4\ M_{\odot}$ (*open histogram*). The hatched histogram represents the stars exhibiting inner disk emission (primordial or weak) as determined by the IRAC SED slope analysis. *Right*: Disk fraction as a function of stellar mass (from the models of Baraffe et al. 1998) for all disk candidates in NGC 2362 with masses $\leq 1.4\ M_{\odot}$ (*filled circles*). The errors plotted represent simple Poisson statistical uncertainties. Superposed are the primordial disk fraction (*solid line*) and the weak disk fraction (*dashed line*) within each $0.1\ M_{\odot}$ mass bin.

fraction of stars earlier than K6 is $11\% \pm 8\%$, $47\% \pm 12\%$ for types K6–M2, and $28\% \pm 5\%$ for M2–M6 types. The immediate implication is that primordial disk lifetimes are prolonged for the progenitors of solar-mass stars (which at 2–3 Myr possess a spectral type of ~K7). To examine whether this trend is evident in the more evolved cluster NGC 2362, the pre-main-sequence models of Baraffe et al. (1998) are used to derive masses for the suspected cluster members. These models are also employed by Lada et al. (2006), who convert from spectral type to $T_{\rm eff}$ using the subgiant temperature scale of Luhman (1999). Hillenbrand & White (2004) compare masses from seven sets of evolutionary models with dynamically determined masses of pre-main-sequence and main-sequence spectroscopic binaries. Their findings suggest that masses derived using the Baraffe et al. (1998) models are in reasonable agreement with dynamical values. To derive the theoretical masses of the suspected cluster population, we have used two-dimensional spline interpolation to create a dense grid of evolutionary tracks in the $(V - I_{\rm C}, V)$ observational plane, extending in age from 1 Myr to 1 Gyr and in mass from 0.1 to $1.4\ M_{\odot}$. The masses for individual members were then determined by minimizing the differences between their extinction-corrected colors and magnitudes and the predicted values of the interpolated grid.

The resulting mass distribution for all candidate cluster members from Tables 1 and 2 with masses $\leq 1.4\ M_{\odot}$ and with complete IRAC photometry is depicted in Figure 7 (*left*) by the open histogram. The hatched histogram represents the stars exhibiting circumstellar disk emission as determined by the IRAC SED analysis. The distribution of disk-bearing stars extends from the ~1.2 to the $0.2\ M_{\odot}$ bins, with the majority (78%) lying between 0.8 and $0.3\ M_{\odot}$. Shown in Figure 7 (*right*) is the fraction of disk candidates relative to the total number of stars within each $0.1\ M_{\odot}$ bin (*filled circles*) with simple Poisson statistical uncertainties overplotted. Superposed are the fractions of primordial disk candidates (*solid line*) and weak disk candidates (*dashed line*) relative to the total number of stars in each mass bin. At the high-mass extremum the disk fraction steadily declines, caused by a real paucity of infrared excesses (shortward of 8 μm) for stars more massive than $\sim 1.2\ M_{\odot}$. The inclusion of the photometric membership sample from Table 2 almost certainly leads to field star contamination in this analysis, a concern that is somewhat mitigated by focusing solely on the activity/lithium-selected sample of stars from Table 1. Plotting the mass distribution for just those stars in Table 1, however, we find little change in the overall stellar mass distribution of the cluster or the mass distribution of disk-bearing stars.

To compare our results directly with those for IC 348, we bin the cluster members by mass using the approximate boundaries of Lada et al. (2006): $M_* > 1.05\ M_{\odot}$, $1.05\ M_{\odot} \geq M_* > 0.6\ M_{\odot}$, and $M_* \leq 0.6\ M_{\odot}$. At the age of NGC 2362, these mass boundaries roughly correspond to spectral types of earlier than ~K5, K5–M0.5, and later than M0.5, whereas in IC 348 they are earlier than K6, K6–M2, and later than M2. Considering just the activity/lithium-selected cluster membership sample, we find the numbers of stars within each of these three mass bins to be 45, 56, and 88, respectively, and can therefore place upper limits on the primordial disk fraction for each mass bin of $2.2\% \pm 2\%$, $10.7\% \pm 4\%$, and $8.0\% \pm 3\%$. By including the additional photometric membership candidates from Table 2, the total numbers of stars within each of the mass bins increase to 66, 72, and 132, thereby reducing the primordial disk fractions to $1.5\% \pm 1.5\%$, $8.3\% \pm 3\%$, and $5.3\% \pm 2\%$, respectively. Comparing these fractions with those in the younger IC 348, we find a similar peak in the mass bin that includes solar analogs, but the observed decline in primordial disk fraction for lower masses is affected by incompleteness for $M_* \leq 0.3\ M_{\odot}$ (§ 3). The significance level of this result is not high given the small number of primordial disk candidates in NGC 2362, photometric uncertainties, and survey incompleteness. Without distinguishing between classes of disk structure (weak or primordial), Figure 7 (*right*) does clearly demonstrate that the inner disk fraction for the low-mass population ($<1.2\ M_{\odot}$) of NGC 2362 is consistent with the findings of Carpenter et al. (2006) in the similarly aged Upper Scorpius OB association. A range of SED profiles among K- and M-type stars are found by Carpenter et al. (2006), but the typical disk in Upper Scorpius is less luminous than those among the younger (~1–2 Myr) Taurus population (see their Fig. 2), similar to our results here.

8. THE ACCRETION FRACTION OF NGC 2362

Much of our understanding of disk structure and evolution has been derived from observations of dust emission, which is either traced directly by scattered light or inferred from near- and mid-infrared excess emission. From the interstellar gas-to-dust mass

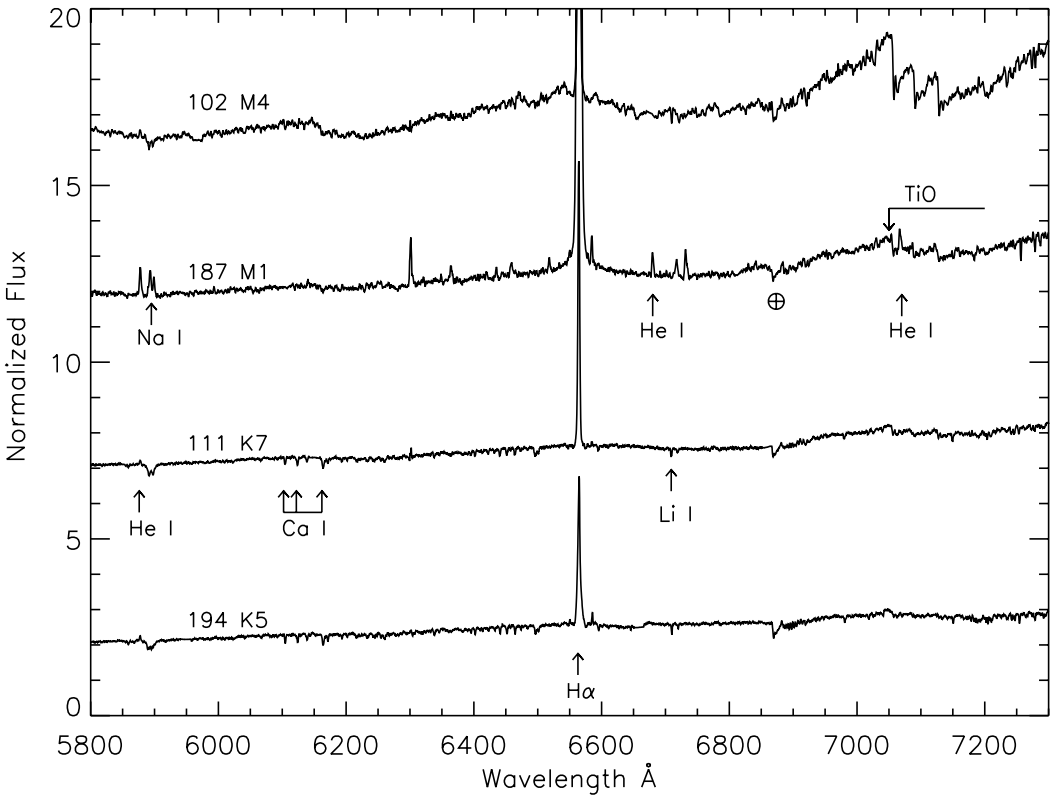

FIG. 8.—GMOS spectra for several suspected accretors in NGC 2362. Of the spectra shown, only the M4-type star 102 lacks infrared excess emission shortward of 5.8 μm. Stars 187 and 111 are primordial disk-bearing candidates, and star 194 is a weak disk system with an IRAC SED slope of $\alpha = -2.49$.

ratio, however, we deduce that primordial disks are initially dominated by molecular gas. At least 0.01 $M_{\odot}$ of H_2 (the minimum mass solar nebula) was required to form the massive envelopes of the giant planets within our own solar system. Given the homonuclear structure of H_2, observed transitions of the molecule are quadrupole in nature and consequently weak. In addition, many of its lines are obscured within regions of poor atmospheric transmission. Even the purely rotational transitions in the mid-infrared require excitation temperatures of several hundred kelvins and significant quantities of gas to produce detectable emission. Given these limitations, accretion is the one indicator of inner disk gas that is readily observable with ground-based instrumentation. In the magnetospheric accretion model, gas from the inner disk is channeled along lines of magnetic flux to the stellar surface. The infalling gas and its subsequent impact are inferred through the broadened profiles of Balmer, He I, and Ca II emission lines (Muzerolle et al. 1998). Mass accretion rates ($\dot{M}$) for members of several nearby SFRs show a steady decline with age, from 10^{-6} to 10^{-10} $M_{\odot}$ yr^{-1} (Gullbring et al. 1998; Hartmann et al. 1998; Muzerolle et al. 2000; Hartmann 2005). This decay occurs over the same approximate timescale as that of optically thick dust emission, but an exact correlation has not been established given the apparent rapid transition from primordial accretion disk to optically thin debris disk. One prominent example of a transition disk is that of the 10 Myr old CTTS TW Hya, which exhibits weak accretion (Muzerolle et al. 2000) but also evidence for inner (0.5 AU) disk clearing (Calvet et al. 2002; Rettig et al. 2004).

The demarcating $W(\mathrm{H}\alpha)$ between CTTSs and WTTSs has traditionally been established at 10 Å, which roughly coincides with the detection threshold of early photographic objective prism surveys. No physical interpretation was intended for this specific equivalent width, but clear phenomenological differences between CTTSs and WTTSs (accreting/chromospherically active) have since been incorporated into their characterizations. The ambiguity of the 10 Å equivalent width and the mass-dependent chromospheric saturation level for Hα emission have led some authors to suggest that the formal definition of CTTSs and WTTSs be spectral type–dependent. Martín (1998), for example, establishes the minimum $W(\mathrm{H}\alpha)$ implying accretion activity to be 5 Å for K-type stars (or earlier), 10 Å for M0–M2 spectral types, and 20 Å for later M types. White & Basri (2003) modify the accretion limits of Martín (1998), proposing that $W(\mathrm{H}\alpha)$ be $\geq$3 Å for K0–K5 stars, $\geq$10 Å for K7–M2.5 spectral types, $\geq$20 Å for M3–M5.5, and $\geq$40 Å for M6–M7.5.

Assuming the classical 10 Å boundary between CTTSs and WTTSs, Lada et al. (2006) find that 68% of the CTTSs in IC 348 are associated with primordial circumstellar disks, another 11% possess weak disks, and the remaining 21% are diskless. Among the WTTS population of IC 348, only 12% retain optically thick disks, 22% are associated with weak disks, and the remaining 66% are diskless. Lada et al. (2006) conclude from these statistics that while infrared excess and accretion are strongly coupled, dust emission persists after gaseous accretion abates. All of the stars in the activity/lithium-selected sample in Table 1 have been examined for Hα emission either with GMOS spectra if available or on the WFGS survey images of Dahm (2005). Assuming the classical definition for CTTSs and WTTSs in NGC 2362, we find that of the 15 CTTSs listed in Table 1, five are associated with primordial, optically thick disks (33%), three are associated with weak disks (20%), three are apparently diskless, and the remaining four have incomplete IRAC photometry. Of these four CTTSs lacking one or more IRAC channels, three can be assessed as nonexcess cluster members based on the fragmentary IRAC data available and the presence of Li I absorption, and one CTTS lacks IRAC photometry altogether, precluding evaluation. Among the 124 WTTSs, 6 are primordial disk candidates (5%), 13 are

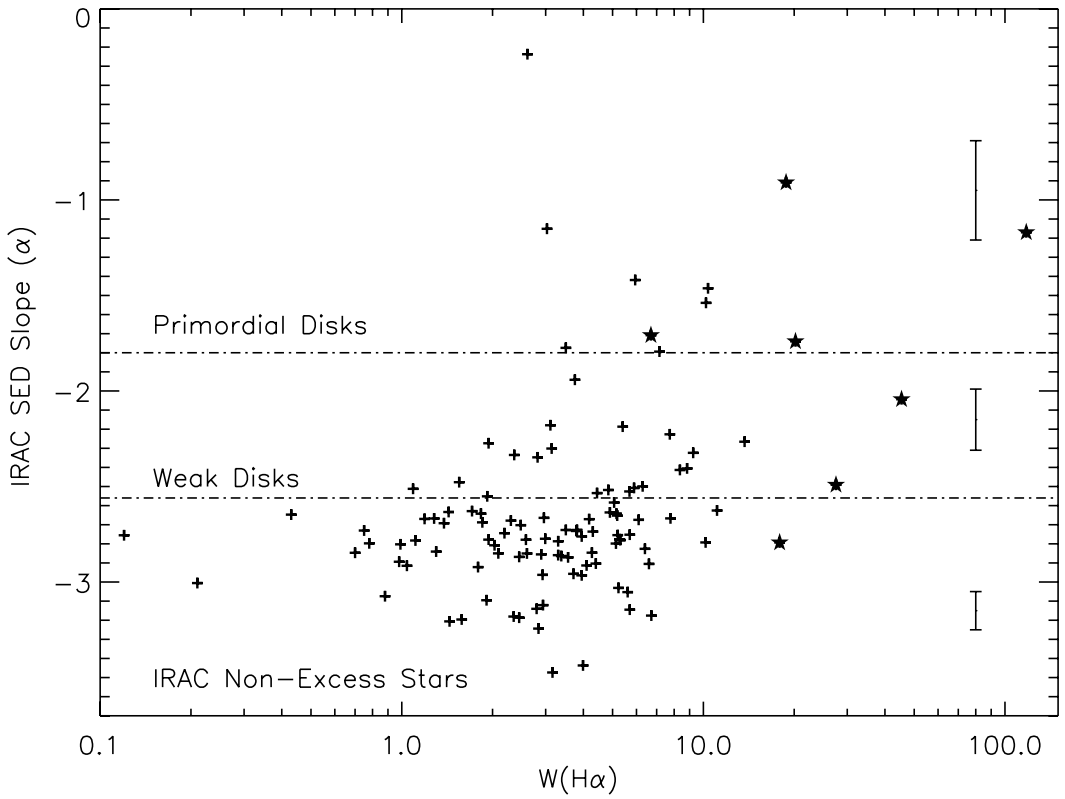

FIG. 9.—IRAC SED slope parameter α plotted as a function of $W(\mathrm{H}\alpha)$ for the Hα-emitting population of NGC 2362. Suspected accretors based on the criteria of White & Basri (2003) are shown as filled stars. A weak positive correlation is present between these parameters, similar to the findings of Lada et al. (2006) for the members of the younger cluster IC 348. Median uncertainties in the IRAC slope parameter α are shown for each disk class and for the IRAC nonexcess stars. The larger uncertainties associated with the disk-bearing candidates arise primarily from their nonlinear SED profiles.

weak disk candidates (10%), 76 are diskless (61%), and the remaining 29 WTTSs lack complete IRAC photometry due to sensitivity limits in one or more channels.

Adopting the spectral type–dependent accretion criteria of White & Basri (2003), we find that only 9 of the 139 Hα emitters in NGC 2362 are likely accretors (stars 12, 38, 78, 85, 102, 111, 187, 194, and 232), from which we infer a lower limit for the cluster accretion fraction of $\sim$4%. Of these nine suspected accretors, four retain primordial disks, two are associated with weak disks, one is diskless, and two have incomplete IRAC photometry but can be assessed as diskless from the channels available. Hα line profiles, however, could not be examined for many of the X-ray-selected stars because of blended or overlapping spectra or the lack of available WFGS data. There are 27 such X-ray-detected stars in Table 1 that lie within the apparent locus of TTSs in the optical color-magnitude diagram. Assuming the same accretion fraction of the detected Hα emitters in NGC 2362 (6.5% using the criteria of White & Basri 2003) to be valid among these 27 stars, we deduce that only two additional accretors should be among them. The accretion fraction of suspected cluster members is thus modified slightly to $\sim$5% $\pm$ 2%. Shown in Figure 8 are the GMOS spectra of four suspected accretors in NGC 2362. Only one of these stars (102) lacks infrared excess (out to 5.8 μm). It is possible that strong chromospheric activity is responsible for the observed Hα emission in this lithium-rich, M4-type star, but follow-up observations are necessary for confirmation.

We plot in Figure 9 the IRAC SED slope parameter α as a function of $W(\mathrm{H}\alpha)$ for all Hα emitters with complete IRAC photometry. In agreement with Lada et al. (2006) for the younger IC 348, we find a weak correlation between the strength of Hα emission and the slope of the IRAC SED. Seven primordial disk candidates lack evidence of accretion activity based on $W(\mathrm{H}\alpha)$, but the shape and strength of Hα emission profiles among accreting TTSs are known to be temporally variable (e.g., Johns & Basri 1995). The relative agreement between the fractions of accreting stars and primordial disk-bearing stars supports the conclusions that inner dust disks and gas disks dissipate over similar timescales. The nonaccreting primordial disks may represent a population of transitional disk systems, but additional spectroscopic observations are needed to confirm the lack of accretion activity. The two weak disk systems suspected of accretion activity are stars 85 and 194 from Table 1. The SEDs of these two suspected accretors are presented in Figure 3 (*right*).

9. IMPLICATIONS FOR CIRCUMSTELLAR DISK EVOLUTION

As more stellar clusters and SFRs are observed with IRAC and MIPS on board *Spitzer*, the frequencies of primordial disks and debris disks as a function of age and stellar mass are unveiling an empirically derived sequence of disk evolution. The methods used to establish the presence of disk emission vary, but the primordial disk fractions determined from the IRAC SED analysis used here and from inspection of the NIR-IRAC ($K_S - 4.5$ μm, $J - H$) color-color diagram yield relatively consistent results. This can be verified by examination of Figure 4 (*right*), which shows that only one of the primordial disk-bearing stars in NGC 2362 recognized by the IRAC SED analysis would definitively not be classified as an inner disk candidate using the ($K_S - 4.5$ μm, $J - H$) color-color diagram. Eight weak disk candidates, however, would be identified as exhibiting optically thick disk emission, suggesting that the primordial disk fraction would likely be overestimated by use of the ($K_S - 4.5$ μm, $J - H$) color-color

diagram alone. Merging results from this analysis of NGC 2362 with those for other young clusters observed by *Spitzer*, we briefly review circumstellar disk evolution from the emergence of the stellar population from its parental molecular cloud to ages of ~10 Myr, when most primordial disks have dissipated.

In the 1–3 Myr old, partially embedded cluster NGC 7129, Gutermuth et al. (2004) use the ($H - 4.5$ μm, $J - H$) color-color diagram to derive an inner disk fraction of 54% ± 14%, suggesting a rapid decline in primordial disk fraction from early ground-based estimates of 86% for the ~1 Myr old population of the Orion Nebula cluster (Lada et al. 2000). The 2–3 Myr old members of IC 348 exhibit a further decline in primordial disk fraction to 30% ± 4%, with another 20% of cluster members retaining weak or transitional disk systems (Lada et al. 2006). In the similarly aged cluster Trumpler 37 (~4 Myr), Sicilia-Aguilar et al. (2006) find that ~38% of the low-mass population retain IRAC excesses indicative of optically thick disk emission, while another 10% exhibit probable emission at wavelengths longer than 4.5 μm. Three intermediate-mass (BAF spectral types) members of Trumpler 37 are also found by Sicilia-Aguilar et al. (2006) to possess optically thick disks, while another three to five such stars exhibit optically thin disk emission. With its well-established age of 5 Myr, an upper limit for the primordial disk fraction of NGC 2362 is placed at ~7% ± 2%, while ~12% ± 3% of suspected members likely retain weak or transitional disks. The frequency of circumstellar disks in NGC 2362 is also strongly mass-dependent, such that no stars more massive than ~1.2 $M_{\odot}$ are found with significant excess emission shortward of 8 μm. Carpenter et al. (2006) find a similar total disk fraction of 19% for the low-mass (0.1–1.0 $M_{\odot}$) members of the 5 Myr old Upper Scorpius OB association, while <1% of more massive stars exhibit primordial disk emission. By ~10 Myr the inner disk fraction diminishes to <4%, the upper limit in NGC 7160 established by Sicilia-Aguilar et al. (2006). All of these young clusters and associations are well populated and presumably representative of the typical birthplaces of most low-mass stars in the Galactic disk.

Perhaps the weakest link in disk evolution studies is the assignment of absolute ages to individual stars or SFRs. The ages and age dispersions of young stellar clusters and associations derived by direct comparison of observed color-magnitude diagrams with various models of stellar evolution are sensitive to photometric uncertainties, unresolved binaries, and intrinsic source variability. The lifetimes of molecular clouds are also disputed as demonstrated by the disparate ages assigned to the Taurus-Auriga molecular cloud complex. Hartmann (2003) argues for rapid star formation within the region, while Palla & Stahler (2002) conclude that star formation has been ongoing within the clouds for at least 10 Myr and possibly as long as 20 Myr. If star formation can be sustained for prolonged periods before cloud dispersal, several generations of stars may be present within a given giant molecular cloud. Acknowledging these caveats, as well as the small numbers of clusters examined thus far by *Spitzer*, we can make some general assertions regarding disk evolution and the formation of planetary systems within the terrestrial region of low-mass stars. Active accretion among a small percentage of members of NGC 2362 suggests that in rare cases, the lifetimes of gas-rich inner disks may exceed the mean primordial disk lifetime by more than a factor of 2. Whether the stars hosting such long-lived accretion disks formed in a later epoch of star formation within the progenitor molecular cloud is uncertain, but two of the accreting primordial disk candidates in NGC 2362 lie near the 10 Myr isochrone in the ($V - I_C$, V) color-magnitude diagram shown in Figure 2. Taken at face value, the isochronal ages for these stars would place them among the oldest members of the cluster. Alternatively, neutral extinction induced by optically thick edge-on disks may account for their inferred low luminosities. Although the steady decline of $\dot{M}$ with age observed in other nearby SFRs occurs over the same approximate timescale as that of optically thick dust emission, the presence of several primordial disk candidates in NGC 2362 with weak Hα emission suggests that inner dust disks may persist after the abatement of gaseous accretion. This is also concluded by Lada et al. (2006) for the younger stellar population of IC 348. Whether trace amounts of gas remain within the inner disks of these apparently nonaccreting stars cannot be assessed without additional observations.

From the summary of *Spitzer*-derived disk frequencies, we can speculate that between ages of ~5 and 10 Myr, the primordial disk fraction of young clusters falls below the observed frequency (6.6%) of giant planets within 5 AU of all FGKM-type stars as determined by high-precision radial velocity surveys (Marcy et al. 2005). Although these *Spitzer* IRAC observations are sensitive to only the inner ~3 AU of disk structure, they do suggest that sufficient numbers of primordial disks persist to ages consistent with the timescale required by core accretion theory to account for the observed frequency of Jovian-like planets around low- and intermediate-mass stars. Additional *Spitzer* IRAC and MIPS observations of minimally evolved clusters (~3–15 Myr) are needed to further examine the terminal phases of primordial disk evolution. Even more critical for the understanding of disk structure and the formation of planetary systems, however, is firm knowledge of the spatial distribution of gas as primordial accretion disks transition to planetary debris disks.

10. SUMMARY

The principal results from this investigation are as follows:

1. Hα emission, Li I λ6708, and *Chandra* ACIS observations of the ~5 Myr old cluster NGC 2362 have identified 232 candidate cluster members, ranging in spectral type from B2 to M5. The suspected members are distributed around τ CMa, the massive O9 Ib multiple star that is centrally located within the cluster core. Optical (VR_CI_C) photometry of the cluster reveals the presence of another ~271 stars lying either on the cluster ZAMS or between the 1 and 10 Myr isochrones of Baraffe et al. (1998) in the ($V - I_C$, V) color-magnitude diagram. Many (~118) of these stars lie below the detection threshold (~0.3 $M_{\odot}$) of the Hα emission and *Chandra* X-ray surveys.

2. Spectral energy distributions have been created for all candidate cluster members from measured fluxes in optical (VR_CI_C), NIR (JHK_S), and *Spitzer* IRAC (3.6, 4.5, 5.8, and 8.0 μm) passbands. Fitting the SEDs to synthetic, low-resolution spectra from the NextGen atmospheric models of Hauschildt et al. (1999), we have identified 47 stars possessing infrared emission in excess of pure stellar photospheres.

3. Acknowledging the limitations of the IRAC SED slope analysis in characterizing disk structure, we use the infrared excess metrics established by Lada et al. (2006) for primordial, weak, and nonexcess stars to establish an upper limit for the primordial disk fraction of NGC 2362 of ~7% ± 2%, while another ~12%± 3% of the suspected cluster members exhibit infrared excess characteristic of weak or optically thin disk emission.

4. The presence of circumstellar disks among candidate members of NGC 2362 is strongly mass-dependent, such that no stars more massive than ~1.2 $M_{\odot}$ exhibit significant infrared excess emission shortward of 8 μm. The mass distribution of disk-bearing stars (primordial and weak) extends from ~1.2 to 0.2 $M_{\odot}$, with the majority (78%) lying between 0.8 and 0.3 $M_{\odot}$. The turnover in disk fraction toward lower masses is very likely an artifact of incompleteness.

5. Dividing the cluster members among three broad mass bins, we find that the primordial disk fraction of candidate members of NGC 2362 peaks near 10.7% $\pm$ 4% for masses between 1.05 and 0.6 $M_{\odot}$. This peak occurs within the same approximate mass range as that found by Lada et al. (2006) in the younger cluster IC 348. The immediate implication is that primordial disk lifetimes are prolonged for the progenitors of solar-mass and less massive stars, thereby permitting more time for the formation of planetary systems within the inner disk regions of these stars.

6. From Hα emission-line strengths and assuming the spectral type–dependent accretion criteria of White & Basri (2003), we find that only 9 of the 139 known Hα emitters in NGC 2362 are likely accretors. Accounting for those stars lacking Hα emission data, we estimate the accretion fraction of suspected cluster members to be $\sim$5% $\pm$ 2%. A weak correlation is also found between the IRAC slope parameter α and the strength of Hα emission among the suspected TTS population of NGC 2362.

This work is based on observations made with the *Spitzer Space Telescope*, which is operated by the Jet Propulsion Laboratory, California Institute of Technology, under NASA contract 1407, the *Chandra X-Ray Observatory*, and the Gemini Multi-Object Spectrograph on Gemini-North. We have made use of the Digitized Sky Surveys, which were produced at the Space Telescope Science Institute under US government grant NAG W-2166, the SIMBAD database operated at CDS, Strasbourg, France, and the Two Micron All Sky Survey, a joint project of the University of Massachusetts and the Infrared Processing and Analysis Center/California Institute of Technology, funded by NASA and the National Science Foundation. We gratefully acknowledge John Carpenter for his sound advice and recommendations for handling *Spitzer* IRAC data and Theodore Simon for reviewing the manuscript and providing many helpful suggestions that improved its quality. S. E. D. is supported by an NSF Astronomy and Astrophysics Postdoctoral Fellowship under award AST 05-02381.

REFERENCES

Balona, L. A., & Laney, C. D. 1996, MNRAS, 281, 1341
Baraffe, I., Chabrier, G., Allard, F., & Hauschildt, P. H. 1998, A&A, 337, 403
Boss, A. 1997, Science, 276, 1836
Calvet, N., D'Alessio, P., Hartmann, L., Wilner, D., Walsh, A., & Sitko, M. 2002, ApJ, 568, 1008
Calvet, N., & Gullbring, E. 1998, ApJ, 509, 802
Carpenter, J. M., Mamajek, E. E., Hillenbrand, L. A., & Meyer, M. R. 2006, ApJ, 651, L49
Dahm, S. E. 2005, AJ, 130, 1805
Everett, M. E., & Howell, S. B. 2001, PASP, 113, 1428
Feigelson, E. D., & Montmerle, T. 1999, ARA&A, 37, 363
Furlan, E., et al. 2006, ApJS, 165, 568
Gullbring, E., Hartmann, L., Briceño, C., & Calvet, N. 1998, ApJ, 492, 323
Gutermuth, R. A., Megeath, S. T., Muzerolle, J., Allen, L. E., Pipher, J. L., Myers, P. C., & Fazio, G. G. 2004, ApJS, 154, 374
Haisch, K. E., Jr., Lada, E. A., & Lada, C. J. 2001, ApJ, 553, L153
Hartmann, L. 2003, ApJ, 585, 398
———. 2005, in ASP Conf. Ser. 341, Chondrites and the Protoplanetary Disk, ed. A. N. Krot, E. R. D. Scott, & B. Reipurth (San Francisco: ASP), 131
Hartmann, L., Calvet, N., Gullbring, E., & D'Alessio, P. 1998, ApJ, 495, 385
Hauschildt, P. H., Allard, F., & Baron, E. 1999, ApJ, 512, 377
Herbig, G. H. 1998, ApJ, 497, 736
Hillenbrand, L. A. 1997, AJ, 113, 1733
Hillenbrand, L. A., Strom, S. E., Calvet, N., Merrill, K. M., Gatley, I., Makidon, R. B., Meyer, M. R., & Skrutskie, M. F. 1998, AJ, 116, 1816
Hillenbrand, L. A., & White, R. J. 2004, ApJ, 604, 741
Johns, C. M., & Basri, G. 1995, AJ, 109, 2800
Johnson, H. L. 1950, ApJ, 112, 240
Kenyon, S. J., & Hartmann, L. 1995, ApJS, 101, 117
Lada, C. J. 1987, in Star Forming Regions, ed. M. Peimbert & J. Jugaku (Dordrecht: Reidel), 17
Lada, C. J., & Lada, E. A. 2003, ARA&A, 41, 57
Lada, C. J., Muench, A. A., Haisch, K. E., Lada, E. A., Alves, J. F., Tollestrup, E. V., & Willner, S. P. 2000, AJ, 120, 3162
Lada, C. J., & Wilking, B. A. 1984, ApJ, 287, 610
Lada, C. J., et al. 2006, AJ, 131, 1574
Lissauer, J. J. 1993, ARA&A, 31, 129
Luhman, K. L. 1999, ApJ, 525, 466
Luhman, K. L., Stauffer, J. R., Muench, A. A., Rieke, G. H., Lada, E. A., Bouvier, J., & Lada, C. J. 2003, ApJ, 593, 1093
Marcy, G., Butler, R. P., Fischer, D. A., Vogt, S. S., Wright, J. T., Tinney, C. G., & Jones, H. R. A. 2005, Prog. Theor. Phys. Suppl., 158, 24
Martín, E. L. 1998, AJ, 115, 351
Martin, P. G., & Whittet, D. C. B. 1990, ApJ, 357, 113
Moitinho, A., Alves, J., Huelamo, N., & Lada, C. J. 2001, ApJ, 563, L73
Muzerolle, J., Calvet, N., Briceño, C., Hartmann, L., & Hillenbrand, L. 2000, ApJ, 535, L47
Muzerolle, J., Hartmann, L., & Calvet, N. 1998, AJ, 116, 455
Natta, A., Testi, L., Calvet, N., Henning, T., Waters, R., & Wilner, D. 2007, in Protostars and Planets V, ed. B. Reipurth, D. Jewitt, & K. Keil (Tucson: Univ. Arizona Press), 767
Palla, F., & Stahler, S. 2002, ApJ, 581, 1194
Rettig, T. W., Haywood, J., Simon, T., Brittain, S. D., & Gibb, E. 2004, ApJ, 616, L163
Sicilia-Aguilar, A., et al. 2006, ApJ, 638, 897
Siegler, N., Muzerolle, J., Young, E. T., Rieke, G. H., Mamajek, E. E., Trilling, D. E., Gorlova, N., & Su, K. Y. L. 2007, ApJ, 654, 580
Silverstone, M. D., et al. 2006, ApJ, 639, 1138
Tokunaga, A. T. 2000, in Allen's Astrophysical Quantities, ed. A. N. Cox (4th ed.; New York: Springer), 143
Tonry, J., Burke, B. E., & Schechter, P. L. 1997, PASP, 109, 1154
White, R. J., & Basri, G. 2003, ApJ, 582, 1109
Zuckerman, B., Song, I., Bessell, M. S., & Webb, R. A. 2001, ApJ, 562, L87